Fragmentation channels of large multicharged clusters

Isidore Last, Yaakov Levy,[a] and Joshua Jortner[b]
School of Chemistry, Tel Aviv University, Ramat Aviv, 69978 Tel Aviv, Israel

(Received 6 May 2005; accepted 15 August 2005; published online 14 October 2005)

We address unifying features of fragmentation channels driven by long-range Coulomb or pseudo-Coulomb forces in clusters, nuclei, droplets, and optical molasses. We studied the energetics, fragmentation patterns, and dynamics of multicharged $(A^+)_n$ ($n=55$, 135, 321) clusters. In Morse clusters the variation of the range of the pair-potential induced changes in the cluster surface energy and in the fissibility parameter $X=E(\text{Coulomb})/2E(\text{surface})$. X was varied in the range of $X=1-8$ for short-range interactions and of $X=0.1-1.0$ for long-range interactions. Metastable cluster configurations were prepared by vertical ionization of the neutral clusters and by subsequent structural equilibration. The energetics of these metastable ionic clusters was described in terms of the liquid drop model, with the coefficients of the volume and surface energies depending linearly on the Morse band dissociation energy. Molecular-dynamics simulations established two distinct fragmentation patterns of multicharged clusters that involve cluster fission into a small number of large, multicharged clusters for $X<1$ and Coulomb explosion into a large number of individual ions and small ionic fragments for $X>1$. The Rayleigh instability limit $X=1$ separates between spatially anisotropic fission and spatially isotropic Coulomb explosion. Distinct features of the fragmentation energetics and dynamics were unveiled. For fission of $n=55$ clusters, large kinetic and internal energies of the large fragments are exhibited and the characteristic fragmentation time is ~700 fs, while for Coulomb explosion the major energy content of the small fragments involves kinetic energy and the characteristic fragmentation time of ~300 fs is shorter. The Rayleigh ($X=1$) limit, leading to isotropic Coulomb explosion, is transcended by a marked enhancement of the Coulomb energy, which is realized for extremely ionized clusters in ultraintense laser fields, or by a dramatic reduction of the surface energy as is the case for the expansion of optical molasses. © *2005 American Institute of Physics*. [DOI: 10.1063/1.2052567]

I. INTRODUCTION

Since the advent of cluster science in the 1970s,[1,2] cluster chemical physics explored the structure, energetics, spectroscopy, and chemical reactivity of clusters focusing on the energy landscapes, spatial structures and shapes, phase changes, superfluidity, energetics, nuclear and electronic level structure, magnetism, vibrational-electronic excitations, response, nuclear-electron dynamics, and reactivity of large finite system.[3–8] The implications and applications of cluster science pointed towards several significant directions. First, size-scaling laws for large clusters provided bridging between finite systems and the corresponding condensed phase.[8–11] Second, specific size effects for small clusters manifested quantum, optical, and chemical effects.[9,12,13] Third, clusters serve as precursors for nanostructures.[14,15] Fourth, finite chemically bound systems and their complexes with water constitute building blocks for biological systems.[16]

The fragmentation of multiply charged clusters driven by long-range Coulomb forces[17–61] bears close analogy to Coulomb instability of nuclei,[62–66] droplets,[67–70] and pseudo-Coulomb instability of optical molasses.[71] These multicharged (or effectively charged), large finite systems span a broad size domain of 10–12 orders of magnitude from femtometer structures of nuclei[62–66] to nanometer structures of large molecules and clusters, to micrometer structures of irradiated ultracold gases,[71] and to millimeter structures of droplets.[68–70] In general, Coulomb instability is due to the repulsion between two or more positive charges. For nuclei, the total charge is roughly proportional to the total number of nucleons, so that the Coulomb stability of nuclei decreases with increasing their size, setting limits to the maximal size of a stable nucleus.[62–66] Heavy nuclei on the verge of energetic stability manifest the fission decay channel, which is described in terms of the liquid drop model (LDM).[64,66,67] The LDM predicts that Coulomb instability of nuclei, with respect to fission, will increase as Z^2/n, where Z is the total charge and n is the number of particles with Z, increasing (approximately linearly) with increasing n. In the nanoscale world, multicharged clusters manifest Coulomb instability[37] with one mode of decay involving cluster fission. This has been detected in doubly charged elemental van der Waals clusters,[17–21,29] molecular clusters,[17,26] and in metal clusters.[17,23,25,26,28,31,33,36–41,53,54] Indeed, for doubly charged clusters, fission has been well described by the LDM.[32,37–40] However, the instability parameters Z^2/n for doubly charged clusters ($Z=2$) decrease with increasing n in an opposite

[a]Present address: Department of Physics, 6230 Urey Hall, University of California at San Diego, 9500 Gilman Drive, La Jolla, California 92093-0371.
[b]Electronic mail: jortner@chemsg1.tau.ac.il

trend as those for nuclei. There are some other quantitative differences between Coulomb instability of clusters and nuclei. A molecular cluster is usually charged by vertical ionization of the neutral cluster, which provides the initial configuration for the fragmentation process. For elemental clusters the ion-neutral atom interaction is stronger than between neutral particles due to covalent and polarization forces. These interactions, which result in the formation of diatomic molecular ions, were shown to significantly affect the decay process in the doubly charged elemental clusters.[33] In metal clusters the ionization effects on the interatomic interactions are of less importance, at least when a small portion of atoms is ionized ($Z \ll n$).[37] The decay of doubly charged metal clusters contributes to the variety in the decay products, which can correspond not only to two ionized clusters (real fission) but also to the production of separated atoms, dimers, or trimers (evaporation).[37,53] The fission of multicharged metal clusters with $Z \ll n$, such as the doubly charged ($Z=2$) clusters, are well described by the LDM.[34] However, in multicharged clusters with $Z>2$, the fragmentation process becomes more diverse than for $Z=2$ clusters because of a large number of accessible channels. The triply charged elemental clusters[19,24] and molecular clusters[17,18] decay to three singly charged ($Z=1$) clusters. The decay products of multicharged metal clusters exhibit not only $Z=1$ clusters, but also multicharged $Z>1$ clusters.[34,37,40,41]

A dramatic enhancement of the ionization level of clusters, up to $Z \sim n$ or $Z \gg n$, was accomplished by extreme multielectron ionization in ultraintense laser fields (peak intensity $I=10^{15}$–10^{20} W cm^{-2}).[42,43,45–52,57–61,72–79] The multielectron ionization mechanism of clusters is distinct from that of a single constituent. It involves three sequential-parallel processes of inner ionization (due to the barrier suppression mechanism for each constituent in the composite laser and inner field), nanoplasma formation and response (involving an energetic plasma of 100 eV–1000 eV confined to the cluster vicinity and responding to the laser field), and outer ionization (induced by barrier suppression for the entire cluster and quasiresonance laser-nanoplasma coupling effects).[44–49,56–61,80] Coulomb instability of a highly charged cluster triggers simultaneous and concurrent Coulomb explosion. From the foregoing discussion of the Coulomb instability of multicharged clusters, we infer that the fragmentation of clusters provides a broad spectrum of fragmentation phenomena from fission to Coulomb explosion, in contrast to nuclei where the fission channel dominates. It will be interesting to establish unifying concepts of the characterization of the fragmentation channels of multiply charged finite systems[81] driven by long-range Coulomb (or pseudo-Coulomb) forces, i.e., clusters,[17–61,72–79] nuclei,[62–65] droplets,[67–70] and optical molasses.[71]

Ubiquitous fragmentation phenomena in multicharged, large finite systems rested on the traditional LDM,[26,30,37,67] where a classically charged drop deforms through elongated shapes to form separate droplets. The fissibility parameter $X=E(\text{Coulomb})/2E(\text{surface})$ characterizes the relative contribution of repulsive (Coulomb) and cohesive (surface) energies to the fission barrier separating between the bound initial states and the fission products. For $X<1$, thermally activated fission over the barrier prevails. At the Rayleigh instability limit of $X=1$ the barrier height is zero.[26,30,37] Many features of nuclear and metal cluster fissions require that quantum shell effects[37] be accounted for. Nevertheless, the simple LDM expression $X=Z^2e^2/16\pi\gamma R_0^3 = (Z^2/n)/(16\pi\gamma r_0^3/e^2)$ (where γ is the surface tension, Z is the total charge, $R_0=r_0n^{1/3}$ is the system's radius, and r_0 is the constituent radius) provided the conceptual framework for the fission of charged finite systems. All these fragmentation phenomena were realized for fissibility parameters below the Rayleigh instability limit of $X=1$, i.e., nuclear fission,[62–66] the fission of elemental and molecular clusters,[17–21,26,29,33] of metal clusters,[17,23,25,26,28,31–33,36–39,41,53,54] and of hydrogen-bonded droplets.[68–70] Above the fissibility limit ($X>1$) barrierless fission and other dissociative channels open up.[37] We shall transcend the Rayleigh instability limit ($X=1$) for Coulomb instability of large finite systems and demonstrate the prevalence of a qualitatively different fragmentation pattern of Coulomb explosion. A preliminary report of that work was already provided.[81] On the basis of molecular-dynamics simulations we shall explore the fragmentation patterns and dynamics of highly charged Morse clusters by varying the range of the pair potential and of the fissibility parameters. The instability of multicharged Morse clusters, which we shall explore, directly reflects on covalent or dispersion-bound chemical and biophysical finite systems. We shall establish the implications of these results for the energetics and dynamics that stem from the distinct fragmentation modes of multicharged, large finite systems.

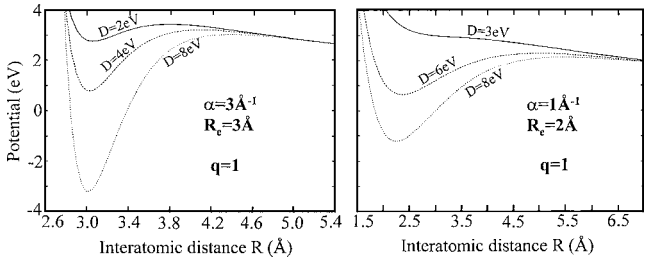

FIG. 1. Pair potentials for charged Morse clusters. The potential parameters for a short-range potential ($\alpha=3$ Å^{-1}, $R_e=3$ Å, $q=1$) and for a long-range potential ($\alpha=1$ Å^{-1}, $R_e=2$ Å, $q=1$) are marked on the panels. The dissociation energy parameters are marked on the curves.

II. MULTICHARGED MORSE CLUSTERS

A. Potential parameters

We studied the energetics, fragmentation patterns, and dynamics of highly charged Morse $(A^+)_n$ clusters consisting of singly charged A^+ ions. The interionic pair potential

$$U(R) = U_M(R) + U_C(R) \tag{1}$$

consists of a Morse potential $U_M(R)$ and a Coulomb repulsive potential $U_C(R)$ (Fig. 1). The interionic attractive Morse pair potential is

$$U_M(R) = DG(G-2) \tag{2}$$

with

$$G = \exp[-\alpha(R - R_e)], \tag{2a}$$

where the potential parameters are the dissociation energy D, the range parameter α, and the equilibrium distance R_e. The Coulomb pair potential is

$$U_C(R) = \bar{B}e^2/R, \tag{3}$$

where $\bar{B}=14.39$ eV Å. The pair-potential parameters for the charged Morse clusters (Fig. 1) were varied in the range of $\alpha=1$–3 Å^{-1}, $R_e=2$–3 Å, and $D=1$–15 eV. Two sets of Morse-potential parameters were considered:

Short-range Morse pair potentials (s) with $\alpha=3$ Å^{-1} and $R_e=3$ Å, where $\alpha R_e=9$, with the Morse pair interactions being predominantly between nearest neighbors and the interaction between non-neighboring atoms being negligibly small. Long-range Morse pair potentials (ℓ), which are still of short range as compared with the Coulomb potential. The Morse-potential parameters were taken as $\alpha=1$ Å^{-1} and $R_e=2$ Å, where $\alpha \mathrm{R_e}=2$, and the contribution of the Morse interactions between non-neighboring atoms is of significance.

The interionic Morse-Coulomb pair potential $U(R)$, Eqs. (1)–(3), is purely repulsive for dissociation energies D, which are smaller than some limiting values $D_0(\alpha,R_e)$, i.e., $D<D_0(\alpha,R_e)$, and exhibit a minimum and a barrier for $D>D_0(\alpha,R_e)$. An estimate for the upper limit of D_0 can be obtained from the simple analysis for the attainment of a minimum at some value $R>R_e$ of the pair potential, Eqs. (1)–(3). From the condition $dU/dR=0$ one can derive an expression for G, Eq. (2a), which is real provided that $D>2\bar{B}e^2/\alpha R^2$ at $R=\bar{R}_m$. Thus the limiting value for the dissociation energy is given by

$$D_0 \cong 2\bar{B}e^2/\alpha\bar{R}_m^2, \tag{4}$$

where $\bar{R}_m(>R_e)$ is the distance for the minimum of the potential curve on the verge of stability. For short-range interactions, type (s), we find that $\bar{R}_m \simeq R_e$, while for long-range interactions, type (ℓ), we find that $\bar{R}_m > R_e$.

For the short-range Morse-Coulomb potential, type (s), we took $\bar{R}_m \simeq 3.0$ Å$=R_e$ and Eq. (4) results in $D_0=1.02$ eV, in accord with the numerical result of $D_0=1.0$ eV obtained from a direct numerical calculation for this set of parameters. In the interval $1.0<D_0<5.8$ eV, the pair potential $U(R_m)$ is positive at its minimum point (R_m), which implies the existence of a metastable state. Stable states with $U(R_m)<0$ are realized for $D>5.8$ eV (Fig. 1). For these stable states the potential barrier is high. For example, at $D=8$ eV, Eqs. (1)–(3) give $\bar{R}_m=3.04$ Å and the potential at the minimum is $U(R_m)=-3.2$ eV [with $U_c(\bar{R}_m)=4.5$ eV and $U_M(\bar{R}_m)=-7.7$ eV], while the maximal energy of $U(R)$ is $U_b=3.0$ eV, resulting in a barrier height of $[U_b-U(\bar{R}_m)]=6.2$ eV (Fig. 1). At $R>4.6$ Å the potential curves for the short-range potential coincide in the range $D=2$–8 eV (Fig. 1), resulting in a negligibly small contribution of the Morse potential, with the pair potential being dominated by the repulsive Coulomb interaction in that region.

The pair-potential curves for the long-range Morse-Coulomb potential of type (ℓ) are presented in Fig. 1. In this case, the minimum on the verge of stability is found to be $\bar{R}_m=2.9$ Å, being considerably larger than $R_e=2$ Å. Equation (4) then results in $D_0=3.4$ eV for the minimal value of the dissociation energy for sustaining a bound state. The Morse potential stops to contribute to the pair potential only at large distances of $R>6.5$–7.0 Å, manifesting the long-range nature of the attractive Morse interactions. The maximal energies U_b for case (ℓ) do not appreciably differ from those for case (s). However, the barrier heights $[U_b-U(\bar{R}_m)]$ are considerably lower for the long-range potential than for the short-range potential (Fig. 1) due to higher values of $U(\bar{R}_m)$ in the former case.

To conclude this presentation of the Morse-Coulomb pair potentials, we note that for multicharged Morse clusters, the absolute values of the attractive and repulsive interactions are comparable. For example, for the short-range Morse-potential parameters [class (s)] of $\alpha=3$ Å^{-1} and $R_e=3$ Å together with $D=4.0$ eV, the Coulomb- and Morse-potential contributions at the equilibrium separation $R_m=3.04$ Å are $U_C(R_m)=4.7$ eV and $U_M(R_m)=-5.5$ eV. This feature of the energetics of multicharged clusters is distinct from that of the nuclei, where the contribution of the repulsive Coulomb potential is considerably smaller than the contribution of the attractive internucleon potentials, and where the repulsion is mainly provided by the kinetic energy of the nuclear motion, which is of quantum origin.[66] On the other hand, in multicharged clusters the motion of the ions is essentially of thermal origin and the contribution of this motion to the energetics of the finite system is considerably smaller than the contribution of the Coulomb repulsion in the temperature domain of $T \simeq 1000$–3000 K. Thus for $T=1000$ K, $k_BT=0.09$ eV, with the thermal energy being considerably smaller than the characteristic energy of several eV for the Morse and Coulomb components of the pair potential.

B. Methodology of simulations

We applied classical (constant energy) molecular-dynamics (MD) simulations to study the energetics, stability, fragmentation channels, and time-resolved decay dynamics of multicharged $(A^+)_n (n=55-321)$ clusters. The mass of each A^+ ion is 100 amu, its charge is $q=1$, and the total cluster charge is $Z=n$. The pair potentials $U(R_{ij})$ were specified in Sec. II A. The total potential energy (Fig. 2) of the multicharged $(A^+)_n$ clusters was taken as

$$E = \Sigma_{i<j}\Sigma U(R_{ij}) \tag{5}$$

which, according to Eqs. (1)–(3), consists of a repulsive Coulomb component $E_C=\Sigma_{i<j}\Sigma U_C(R_{ij})$ and an attractive Morse component $E_M=\Sigma_{i<j}\Sigma U_M(R_{ij})$, so that the total potential energy is

$$E(\{R_{ij}\}) = E_C(\{R_{ij}\}) + E_M(\{R_{ij}\}). \tag{5a}$$

The equilibrium icosahedral structures of the neutral $(A)_n$ clusters, with the "magic" numbers $n=55$, 135, 321, were determined by simulated annealing for the energy minimization. These neutral clusters were vertically ionized (at their initial icosahedral structure) to form multicharged $(A^+)_n$ clus-

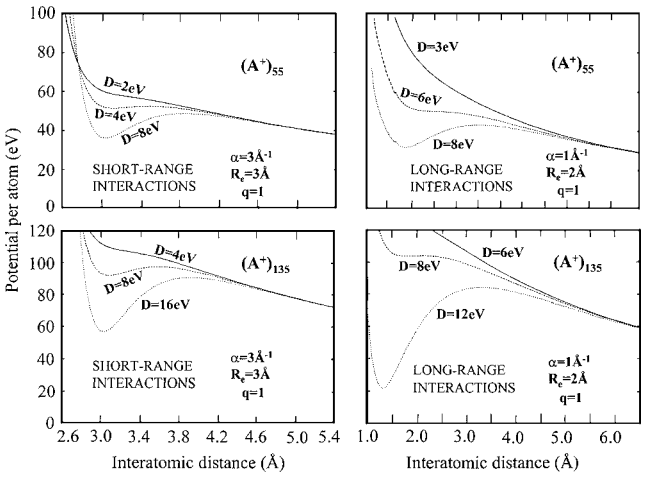

FIG. 2. Energy landscapes for the radial expansion of $(A^+)_{55}$ clusters (the two top panels) and of $(A^+)_{135}$ clusters (the two bottom panels). The potential parameters for short-range and for long-range interactions are marked on the panels. The dissociation energy parameters are marked on the curves. Note that all the minima in the potential surfaces correspond to metastable states.

ters. The energetic data for the Morse-Coulomb clusters will be presented in Secs. II C and III.

Fragmentation dynamics of $(A^+)_n$ (n=55, 135, 321) was explored by molecular-dynamics simulations. The multicharged cluster was initially prepared in a nuclear configuration which corresponds to a vertically ionized state and moved by an equilibration procedure to a nuclear configuration which corresponds to the minimum potential energy of the metastable configuration (Sec. II C). Thermal excitation was obtained by a temperature jump to temperature T. The initial t=0 nuclear configuration of the multicharged cluster is presented in the geometry of the zero-temperature cluster, with a thermal, Maxwell distribution of the velocities of the atoms, which corresponds to the temperature T. This thermal excitation by a "temperature jump" involves complete intramolecular vibrational relaxation (IVR) within the ionic cluster. The dynamic results from the molecular-dynamics simulations will be presented in Sec. IV.

C. Energetic stability of multicharged clusters

Potential-energy landscapes for the $(A^+)_n$ charged clusters, which were calculated per atom

$$E(\{R_{ij}\})/n = E_C(\{R_{ij}\})/n + E_M(\{R_{ij}\})/n, \tag{5b}$$

are displayed in Fig. 2. $E(\{R_{ij}\})/n$ is presented as a function of the interatomic distances, where we took $R_{ij}=R$ for all nearest-neighbor distances i and j. The Morse component in Eq. (5b) contributes to the cluster binding, i.e., $E_M/n<0$ at all band distances R, except for the short interionic distances of $R<R_e-(\ell n 2/\alpha)$, where the Morse component $E_M/n(>0)$ also provides a repulsive contribution. An energetically stable configuration of the $(A^+)_n$ cluster will exist provided that its energy is negative, being lower than the energy of the products in any decay channel, i.e., evaporation, fragmentation, etc. The $(A^+)_n$ clusters may also exist in a metastable configuration, with E being higher than the total energy of the products in some decay channels but separated from them by a barrier (Fig. 2). In particular, the energy of the metastable configuration of the clusters is positive, i.e., $E>0$ (Fig. 2), in analogy to the case of diatomic doubly charged A_2^{2+} ions (Fig. 1). We shall consider the stability or metastability of a cluster at T=0 and in the absence of noticeable quantum effects. We then introduce a limiting value $D_L(\alpha,R_e,n)$ for the dissociation energy in the pair potential, which provides a stable or metastable configuration of the $(A^+)_n$ cluster for $D>D_L(\alpha,R_e,n)$. In the case of short-range Morse pair potentials (with α=3 Å^{-1}, R_e=3 Å), we find the limiting values D_L=4.2 eV for n=55, D_L=8.1 eV for n=135, and D_L=14.2 eV for n=321. In the case of long-range pair Morse potentials (with α=1 Å^{-1}, R_e=2 Å), the limiting values are D_L=6.5 eV for n=55, D_L=8.2 eV for n=135, and D_L=9.6 eV for n=321. For the case of the short-range potential the size dependence of the limiting value is of the form $D_L \propto n^{2/3}$ in analogy to the size dependence of the Coulomb energy per ion (E_C/n), which will be discussed in Sec. III. On the other hand, in the case of the long-range pair potential, the dependence of D_L on n is considerably weaker than for the previous case. All the cluster potential energies of equilibrium configurations at a minimum energy of $D>D_L$ for the potential parameters of classes (s) and (ℓ), which are presented in Fig. 2, are positive ($E>0$) corresponding to a metastable state.

III. THE LIQUID DROP MODEL FOR THE ENERGETICS OF MORSE-COULOMB CLUSTERS

The potential energies of the multicharged metastable $(A^+)_n$ clusters (n=55, 135, 321) at the metastable state, which correspond to the minimum of the potential surface, were analyzed by the LDM.[37,66] In the usual presentation of the LDM one considers the binding energies (per particle). In what follows we shall analyze the potential energies (per ion), which are taken relative to the reference state of separated ions. All energies will be given per particle. The potential energy $\epsilon=E/n$, where E is given by Eq. (5), is

$$\epsilon = \epsilon_C + \epsilon_M, \tag{6}$$

where

$$\epsilon_C = a_c n^{2/3} \tag{7a}$$

is the Coulomb energy. The Morse energy is

$$\epsilon_M = \epsilon_S + \epsilon_V, \tag{7b}$$

where the surface energy is $\epsilon_S=a_s n^{-1/3}$, while the interior energy is $\epsilon_V=a_v$. Equation (6) is then given in the form

$$\epsilon = a_c n^{2/3} + a_v + a_s n^{-1/3}. \tag{7c}$$

Here the parameters a_c, a_v, and a_s are size independent. The input data for the LDM analysis were obtained from the numerically calculated values of ϵ and of ϵ_C, at the equilibrium cluster configuration, taking $\epsilon_M=\epsilon-\epsilon_C$, so that

$$\epsilon_M = a_s n^{-1/3} + a_v. \tag{7d}$$

The size dependence of ϵ_C and ϵ_M for the metastable ionic cluster configuration was calculated for the short-range Morse pair potential (s) with D=14.2 eV and for the long-range Morse pair potential (ℓ) with D=9.6 eV (Fig. 3).

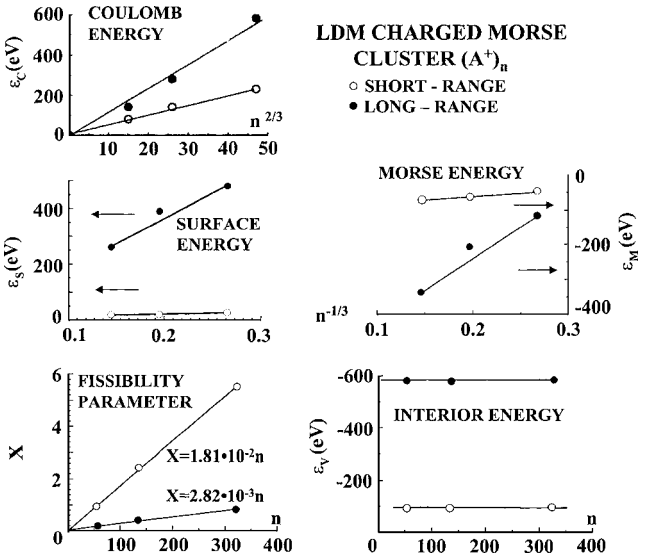

FIG. 3. Analysis of the energetics of the icosahedral charged $(A^+)_n$ (n=55, 135, 321) Morse clusters prepared by vertical ionization of the corresponding neutral clusters. The potential parameters are (s) short-range potential with δ=3 Å^{-1}, R_e=3 Å, D=14.2 eV, and q=1 (O); (ℓ) long-range potential with α=1 Å^{-1}, R_e=2 Å, D=9.6 eV, and q=1 (●). All energies are given per particle. The Coulomb energy is $\in_C = a_c n^{2/3}$, the surface energy is $E_S = a_s n^{-1/3}$, the Morse energy is $\in_M = a_v + a_s n^{-1/3}$, the interior energy is independent of n, and the fissibility parameter is $X \propto n$.

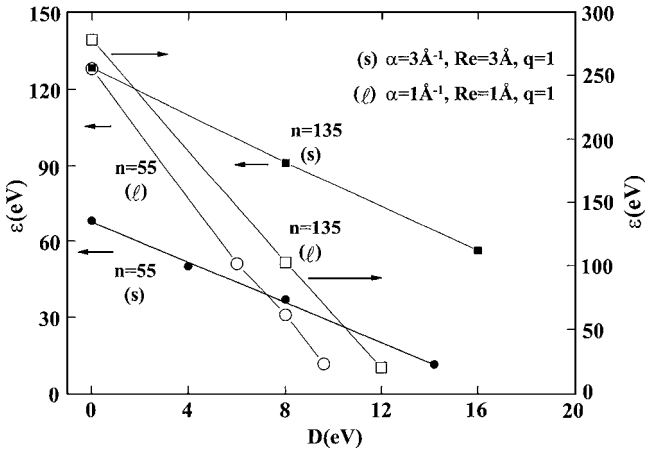

FIG. 4. Linear dependence of the potential energy per ion $\in$ on the Morse-potential dissociation energy D for the equilibrium metastable configuration of $(A^+)_n$ (n=35, 135) clusters for the (s) and (ℓ) potential parameters displayed on the figure. The Coulomb energies $\in_C$ at D=0 were presented for each cluster. ● (s)n=55, ○ (ℓ)n=55, ■ (s)n=35, □ (ℓ)n=135.

These D parameters correspond to the D_L limiting values (Sec. II C) for the largest size (n=321) clusters. From the plots of ϵ_C vs $n^{2/3}$, according to Eq. (7a), the parameters a_c were estimated, while the plot of ϵ_M vs $n^{-1/3}$, according to Eq. (7d), resulted in the estimates of the parameters a_s and a_v (Fig. 3). From the analysis the parameters a_c, a_v, and a_s are inferred for the short-range and the long-range Morse pair potentials and are summarized in Table I.

An important parameter in the LDM is Rayleigh's fissibility parameter, which can be expressed as

$$X = \epsilon_C / 2\epsilon_S. \tag{8}$$

A coarse-grained value of X is obtained from the data relation

$$X = (a_c / 2a_s) n. \tag{8a}$$

It follows from Eq. (8a) that X is proportional to n, in accord with the relation $X \propto Z^2/n$ (Sec. I), whereas in our case $Z = n$ and $Z^2/n = n$. The one order of magnitude difference between the a_s parameters and the close proximity (within a numerical factor of 2) for the two a_c parameters in Table I implies that the fissibility parameter for a given cluster size is considerably lower for the (ℓ) potential than for the (s) potential. The proportionality parameters $X = bn$ with $b = a_c/2a_s$ are given in Table I for the (s) parameters with $\alpha = 3$ Å^{-1}, R_e=3 Å, and D=14.2 eV and for the (ℓ) parameters with α=1 Å^{-1}, R_e=2 Å, and D=9.6 eV.

We now consider the dependence of the total potential energy ϵ, Eqs. (7a) and (7b), on the Morse-potential dissociation energy D and will subsequently extend these results to obtain an empirical cluster size equation accounting for the dependence of ϵ on D and on n. To assess the dependence of ϵ on D at a fixed value of n, we have taken the energetic data at the minima of the energy landscapes (Fig. 2) and the data of ϵ from Fig. 3. In Fig. 4 we portray the ϵ data for $(A^+)_n$ (n=55 and 135) clusters for the (s) potential with α=3 Å^{-1} and R_e=3 Å and for the (ℓ) potential with α=1 Å^{-1} and R_e=2 Å, with the dissociation energy parameters varying over the range D=4–16 eV. These data for n=55 clusters can be fitted by the empirical linear relation

$$\epsilon = A + BD. \tag{9}$$

The parameters A and B are summarized in Table II. From the comparisons between Eq. (7c) and (9) it is apparent that the contribution of the A term in Eq. (9) originates from the Coulomb energy

$$A = \epsilon_C = a_c n^{2/3}, \tag{9a}$$

where the coefficient a_c is independent of D. In Fig. 4 we have also included the values of $\epsilon = \epsilon_C$ and D=0. As is apparent from Table II and Fig. 4, there is a good agreement

TABLE I. Parameters for the LDM fit of the equilibrium potential energies for icosahedral $(A^+)_n$ clusters with n=55, 135, and 321. (s) and (ℓ) are specified in the columns.

	(s) Short-range Morse potential α=3 Å^{-1}, R_e=3 Å, D=14.2 eV, q=1	(ℓ) Long-range Morse potential α=1 Å^{-1}, R_e=2 Å, D=9.6 eV, q=1
a_c(eV)	4.8±0.1	10.8±2
a_v(eV)	−80±1	−600±12
a_s(eV)	132±2	1900±380
$a_c/2a_s$	1.82×10^{-2}	2.84×10^{-3}

TABLE II. Parameters for the cluster size dependence of the potential energy $\in$ and its dependence on D for $(A^+)_n$ clusters at the equilibrium nuclear configuration of the metastable state.

Potential[a]	n	B [b]	A(eV) [b]	$\in_c = a_c n^{2/3}$(eV)	a_v^0 [c]	a_v/D	a_s^0 [c]	a_s/D
(s)	55	-3.79	67	68.1				
(ℓ)	55	-11.3	119	128.0				
(s)	135	-4.56	128	128.3				
(ℓ)	135	-21.5	278	279.1				
(s)	55 and 135				-6.9	-5.6	11.5	9.3
(ℓ)	55 and 135				-50	-42.2	148	198

[a]Potential parameters $(s)\alpha=3$ Å^{-1}, $R_e=3$ Å, $q=1$; $(\ell)\alpha=1$ Å^{-1}, $R_e=2$ Å, $q=1$.
[b]Parameters for the linear fit from Eq. (9).
[c]Parameters from Eq. (9a).

between the values of A and of ϵ_C. Furthermore, the scaling law $A \simeq \epsilon_C \propto n^{2/3}$ is well obeyed (Table II). The differences between the A values for the (s) and (ℓ) potentials are due to the differences in the Morse-potential parameters R_e and α given above, which affect the equilibrium structure and the electrostatic energy in the equilibrium metastable state. The contribution of the B term in Eq. (9) originates from volume and surface contributions to ϵ, with $B=(a_v+a_s n^{-1/3})/D$. Provided that the linear relations $a_v=a_v^0 D$ and $a_s=a_s^0 D$ hold, we obtain

$$B = a_v^0 + a_s^0 n^{-1/3} \tag{9b}$$

which is independent of D. The parameters a_v^0 and a_s^0, Eq. (9b), were evaluated from the B data (Table II) at $n=55$ and at $n=135$ (Table II) being in reasonable agreement with the parameters a_v/D and a_s/D, respectively, which were obtained from the parameters of Table I. In summary, D and the cluster size dependence of ϵ can be represented in the form

$$\epsilon = a_c n^{2/3} + D(a_v^0 + a_s^0 n^{-1/3}), \tag{10}$$

where the parameters a_c, a_v^0, and a_s^0 (Table II) are independent of D and depend on the Morse parameters and on R_e. The generalized size equation (10) will be useful for the assessment of the energy balance in Coulomb explosion and fission, which will be presented in Sec. IV.

From the foregoing analysis, the fissibility parameter, Eqs. (8) and (8a), will be given in the form

$$X = (a_c/2a_s^0 D)n, \tag{11}$$

where a_c and a_s^0 (Table II) are independent of the Morse dissociation energy D but do depend on the parameters α and R_e. Equations (8) and (11) will be used for the classification of cluster fragmentation patterns. The cluster size domain $n=55$–321 studied herein corresponds to $X=0.1$–1.0 for the long-range Morse potential [type (ℓ)] and $X=1$–8 for the short-range Morse potential [type (s)]. Our MD simulations of the fragmentation of multicharged clusters reported in Sec. IV will demonstrate that two major fragmentation patterns are manifested:

(1) For multicharged clusters with $X<1$, which correspond to the (ℓ) potential, cluster fission into a small number of large multicharged clusters takes place. The fission process is spatially anisotropic.
(2) For multicharged clusters with $X>1$, which correspond to the (s) potential, cluster Coulomb explosion into a large number of individual ions and small ionic fragments occurs. The Coulomb explosion process is nearly spatially isotropic. Our molecular-dynamics simulations, reported in Sec. IV, revealed that the qualitative difference in the fissibility parameters between the charged long-range $(X<1)$ and short-range $(X>1)$ Morse potentials induces distinct fragmentation channels driven by the Coulomb instability of these two classes of multicharged clusters.

IV. DYNAMICS OF FISSION AND COULOMB EXPLOSION

We have studied fragmentation channels and decay dynamics of multicharged $(A^+)_n$ Morse clusters, which are metastable at $T=0$, being close to the limit of stability. The D parameter for these clusters is slightly larger than the value of D_L (Sec. II C). Fragmentation from such metastable states is expected to occur at finite temperatures. Molecular-dynamics simulations (Sec. II B) on the time scale of up to 1 ns were carried out, with the multicharged cluster being subjected at $t=0$ to a final temperature of $T=500-10^4$ K and the simulations being performed for a configurationally equilibrated cluster. The fragmentation process

$$(A^+)_n \rightarrow \{A_k^{k+}\}$$

results in the fragments of cluster ions $A_k^{k+}(1 \leqslant k<n)$ of sizes n_k with $\Sigma_k k n_k = n$. Histograms of the ionic products n_k vs k are presented in Figs. 5(a) and 5(b) for the fragmentation of $(A^+)_{55}$ and of $(A^+)_{135}$ Morse-Coulomb clusters. The corresponding values of X, also marked on the histograms, were calculated from Eq. (8).

For the long-range Morse potential $(X<1)$, the clusters fragment into a small number of large, multicharged clusters, which contain the majority of the ions. For $n=55$ with $D=7.0$ eV at $T=10\,000$ K$(X=0.18)$, the clusters fragment into two $(A^+)_{25}+(A^+)_{26}$ clusters and four monoatomic ions, while a similar situation prevails for $n=55$ with $D=6.5$ eV at $T=3000$ K$(X=0.24)$ [Fig. 5(a)]. For $n=135$ with $D=8.2$ eV$(X=0.43)$ fragmentation into three large multicharged clusters occurs. Only a small number of low-sized clusters (e.g., n_1 and n_2) are produced [Fig. 5(b)]. This fragmentation process into a small number of large clusters corresponds to symmetric fission for $n=55$ and asymmetric fission for $n=135$. The general fragmentation pattern for n

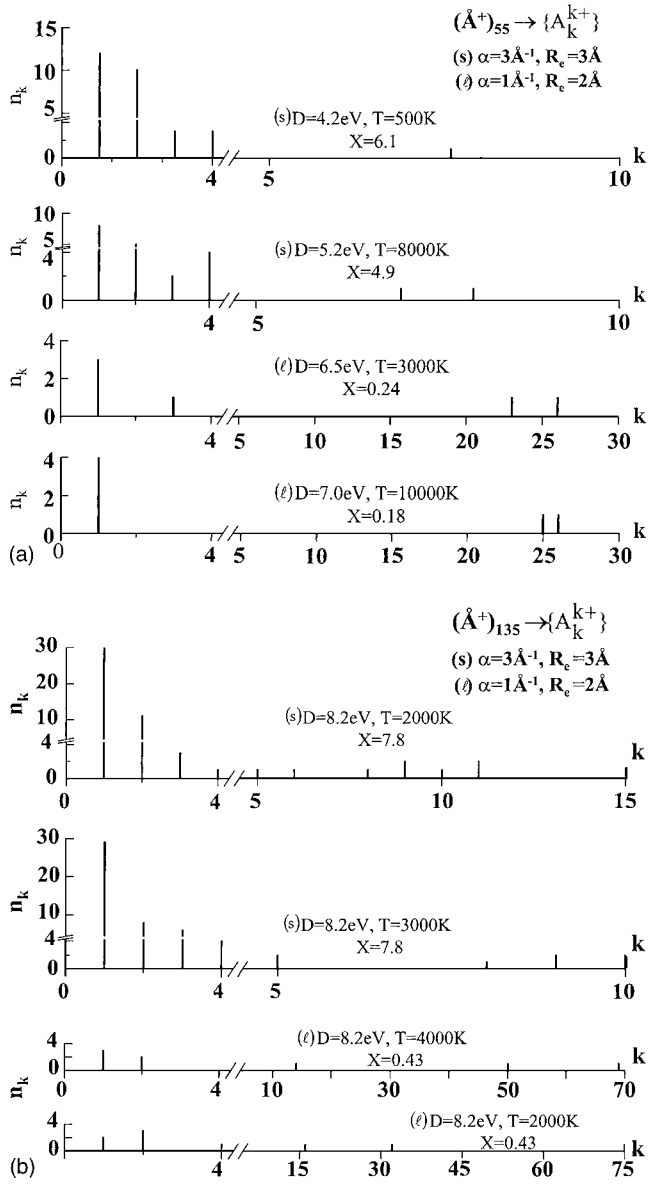

FIG. 5. Fragmentation patterns of multicharged $(A^+)_n$ clusters. The distribution n_k of the ionic fragments $\{A_k^{k+}\}$ is presented by the histograms of the product size. Data are presented for (s) short-range Morse potential $\alpha = 3$ Å^{-1}, $R_e = 3$ Å, $q=1$; (ℓ) long-range Morse potential $\alpha = 1$ Å^{-1}, $R_e = 2$ Å, $q=1$, with the corresponding D and X parameters marked on the figures. Note cluster fission into a small number of large ionic fragments for case (ℓ) and Coulomb explosion into a large number of small ionic fragments for case (s). (a) $n=55$, (b) $n=135$.

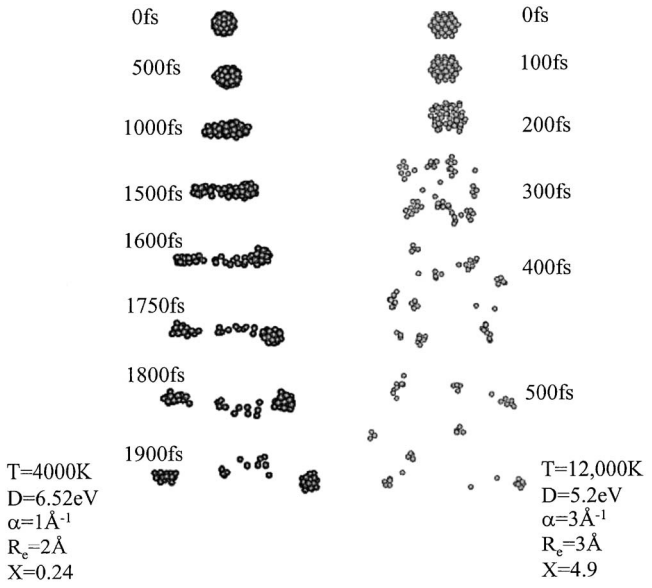

FIG. 6. Snapshots of the fragmentation of highly charged $(A^+)_{55}$ Morse clusters. The potential parameters are marked on the two panels. The right panel corresponds to short-range interactions with $X=1.8$. The left panel corresponds to long-range interactions with $X=0.13$. The transient structures at different times ($T=0$–1500 fs) are marked on each picture. The time $t=0$ corresponds to the T jump of the final temperatures marked on the panels. Note the dramatic distinction between the (spatially isotropic) Coulomb explosion in the upper panel and the (spatially anisotropic) tertiary fission in the lower panel.

$=55$ in the temperature range $T=3000$–$10\,000$ K($X=0.18$–0.24) and for $n=135(X=0.43)$ in the temperature range $T=2000$–4000 K is practically temperature independent.

The situation is qualitatively different for the short-range Morse potential ($X=1.8$ for $n=55$ and $X=4.5$ for $n=135$), where the fragmentation involves a large number of small ionic fragments [Figs. 5(a) and 5(b)]. For example, for $n=135$, $D=8.2$ eV and $T=2000$ K, the multicharged cluster disintegrates into 76 product ions $A_k^{k+}(1 \leqslant k \leqslant 11)$ which contain 11 A_k^{2+} diatomic ions and 31 A^+ atomic ions [Fig. 5(b)]. This fragmentation channel for $X=4.9$–7.8 corresponds to Coulomb explosion. Again, the general fragmentation pattern into a large number of small clusters for $n=55$ in the temperature range $T=500$–8000 K and $n=135(X=7.9)$ in the temperature range $T=2000$–3000 K is weakly temperature dependent [Figs. 5(a) and 5(b)].

The distinction between cluster fission and Coulomb explosion is reflected in the spatial distribution of the charged fragments. This is demonstrated in Fig. 6, where we display the snapshots of the fragmentation of $(A^+)_{55}$ Morse-Coulomb clusters. The most significant qualitative result is that for the long-range Morse potential (ℓ), where $X=0.24$ and where a nearly binary cluster fission is exhibited. This fission process is spatially anisotropic, with the deformation of the parent multicharged cluster via one-axis elongation forming two large clusters (Fig. 6). On the other hand, for the short-range Morse potential (s) $X=4.9$, where the Coulomb explosion process is spatially isotropic with the small ionic fragments expanding radially (Fig. 6).

The energy distribution of the product ionic fragments is displayed in Fig. 7 for the fragmentation of $(A^+)_{55}$ clusters, where we present the kinetic energy E_{KE} and the inner energy E_{IN} of each ionic fragment. Data are presented for a $(A^+)_{55}$ cluster with the short-range Morse potential $(s)\alpha = 3.0$ Å^{-1}, $R_e=3$ Å, $D=4.2$ eV($X=6.1$), and $T=500$ K, and for a cluster with the long-range Morse potential (ℓ) with $\alpha=1$ Å^{-1}, $R_e=2$ Å, $D=6.5$ eV($X=0.24$), and $T=3000$ K. For the fission channel accomplished in the (ℓ) case ($X=0.24$), the kinetic energies of the two large fragments are very high, i.e., $E_{\mathrm{KIN}}=673$ eV for $n=26$ and $E_{\mathrm{KIN}}=757$ eV for $n=23$ [Fig. 7(a)]. The inner potential energies are also very high due to Coulomb repulsion within the large fragments, i.e., $E_{\mathrm{IN}}=590$ eV for $n=26$ and $E_{\mathrm{IN}}=448$ eV for $n=23$ [Fig. 7(a)]. In the latter case the total kinetic energy of the frag-

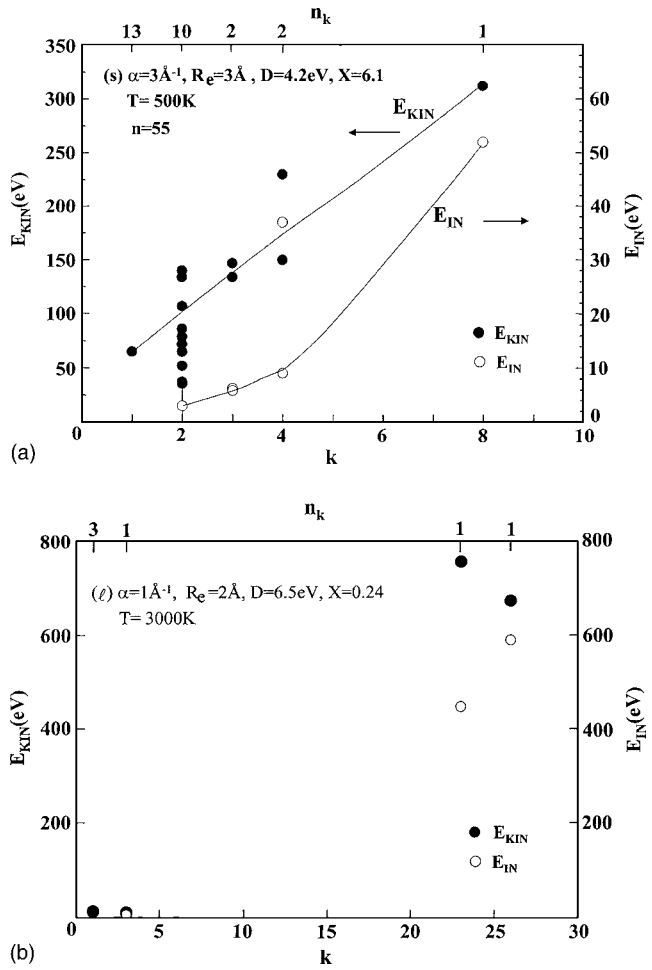

FIG. 7. The distribution of the kinetic energy (E_{KIN}) and the inner potential energy (E_{IN}) of the product ions in the fragmentation of $(A^+)_{55}$ clusters. The fragment size k and abundance n_k are marked on the horizontal upper and lower axes. (a) (s)-type potential parameters $\alpha=3$ Å^{-1}, $R_e=3$ Å, $D=4.2$ eV, $q=1$. Cluster fragmentation at $T=500$ K. The fragmentation involves Coulomb explosion. The spread of the values of E_{KIN} for fixed k is given for $k=8$–2, while the spread of the values of E_{IN} is given for $k=8$–3, with the error bar for $k=2$ marking the spread of these energies. For $k=1$ an average value of E_{KIN} is given. The lines were drawn to guide the eye. (b) (ℓ)-type potential parameters $\alpha=1$ Å^{-1}, $R_e=2$ Å, $D=6.5$ eV, $q=1$. Cluster fragmentation at $T=3000$ K. The fragmentation involves cluster fission into two fragments of $k=26$ and 23, together with a small number of $k=3$ and 1 fragments.

ments is $\Sigma E_{KIN}=1472$ eV while their total inner energy is $\Sigma E_{IN}=1043$ eV, with ΣE_{KE} exceeding ΣE_{IN} by about 40%. For the Coulomb explosion channel accomplished in the (s) case ($X=1.8$), the kinetic energies E_{KIN} of the small fragments considerably exceed their inner energies [Fig. 7(a)], with $\Sigma E_{KIN}=2620$ eV while $\Sigma E_{IN}=140$ eV, with E_{IN} being only 5% of the total product energy. The final energies of the products are summarized in Table III. To assess the energy balance in the fragmentation process, we have calculated the initial potential energies of the metastable states using Eq. (9) together with the dissociation energies D for the Morse potentials. This procedure results in the estimates $\in=50.5$ eV for the (s) potential ($D=4.2$ eV) and $\in=46$ eV for the (ℓ) potential ($D=6.5$ eV). These estimates of $\in$ were used to calculate the initial cluster potential energies (Table III). From the data of Table III we infer that

$$\sum E_{KIN}+\sum E_{IN}=n\in . \tag{12}$$

From Eq. (12) it follows that the energy conservation condition between the initial potential energy of the cluster and the total energy of the fragments is satisfied within the uncertainty range of 2%. The data for $n\in$ are not sufficiently accurate to establish whether fragmentation is governed by thermodynamic constraints, occurring via equilibration between the energy of the minimum of the potential surface and the products, or, alternatively, that it is governed by kinetic constraints, occurring from fragmentation for a transition state. In the case of thermodynamic equilibrium one expects that the initial potential (free) energy on the right-hand side of Eq. (12) will correspond to $n\in$, while in the case of the kinetic situation this energy is given by the transition state energy.

Three points should be made at this stage concerning both fission and Coulomb explosion. First, the kinetic energy E_{KIN} for Coulomb explosion increases with increasing the cluster size, in accord with (divergent) cluster size equations for Coulomb explosion.[60,61] Second, the internal energy of the products also includes rotational energy which is, however, small relative to the Coulomb repulsive energy. Third, the initial potential energies of the polyatomic ions are positive indicating that they exist in a metastable state.

We have also studied the fragmentation of multicharged clusters of the form $(A)_{n1}(A^+)_{n2}$, with $n=n1+n2$ being taken as $n=55$, 135, 321. When $n2/(n1+n2)\geqslant 0.4$, the fragmentation pattern of these clusters is similar to that of the $(A^+)_n$ clusters. Our description of the fragmentation dynamics of multicharged $(X^+)_n$ clusters considered a homogeneous distribution of the charge throughout the cluster volume. Of interest are situations of inhomogeneous initial charge distribution.[59–61] These can be realized in multicharged heteroclusters[61] by the enhancement of inner ionization in elemental clusters [e.g., $(Xe)_n$] induced by ignition effects[59] and by the creation of a persistent nanoplasma within the cluster.[60] The implications of these interesting phenomena of the energetics and dynamics of Coulomb explosion deserve further study.

Some features of time-resolved dynamics of two distinct fragmentation modes emerge from the molecular-dynamics simulations. The time-resolved spatial configurations of multicharged clusters resulting from fission and from Coulomb explosion are presented in Fig. 6. We introduce the cluster fragmentation time τ_F^{η} for the η-fold spatial expansion of the initial cluster radius R_0. τ_F^{η} is defined in terms of the expansion of the fragments (i.e., two large clusters for fission or for the many small fragments for Coulomb explosion) to a boundary size L (measured from the center of the cluster at

TABLE III. Energy balance in the fragmentation $(Ar^+)_n(n=55)$ clusters. Coulomb explosion for (s)$\alpha=3$ Å^{-1}, $R_e=3$ Å, $D=4.2$ eV at $T=500$ K; and fission for (ℓ)$\alpha=1$ Å^{-1}, $R_e=2$ Å, $D=6.5$ eV at $T=3000$ K.

Potential	ΣE_{KE}(eV)	ΣE_{IN}(eV)	$\Sigma E_{KE}+\Sigma E_{IN}$(eV)	$n\in$ (eV)
(s)	2620	140	2760	2778
(ℓ)	1472	1043	2515	2530

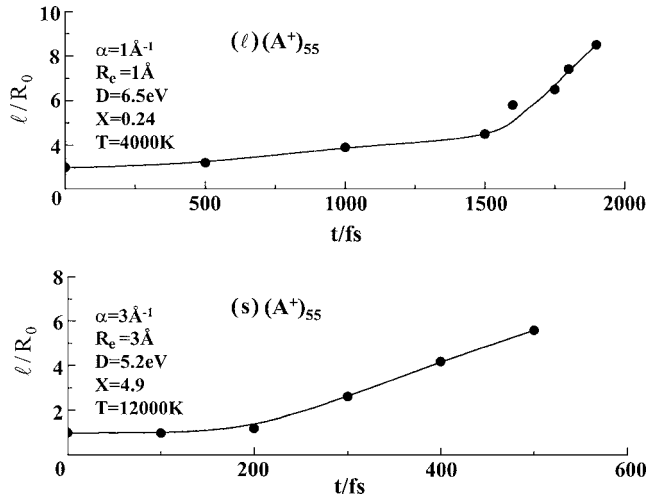

FIG. 8. Time dependence of the cluster spatial expansion in fission and Coulomb explosion of $(A^+)_{55}$ clusters, of ℓ/R_0, where ℓ is the boundary size and R_0 is the initial cluster radius. The upper panel corresponds to fission with a (s) potential, while the lower panel corresponds to Coulomb explosion with a (ℓ) potential. Potential parameters are marked on the panels. The lines were drawn to guide the eye.

$t=0$) with $\eta=L/R_0$. In Fig. 8 we present the time dependence of $\eta=L/R_0$ from the data of Fig. 6. For $(A^+)_{55}$ clusters, the characteristic time scale for Coulomb explosion ($\sim$200–500 fs) is considerably shorter than the time scale for fission ($\sim$1.0–2.0 ps). To provide a semiquantitative estimate of these time scales we define the characteristic times for the doubling of the initial cluster radius, i.e., $t_F^{\eta=2}$ (for $\eta=L/R_0=2$). For $(A^+)_{55}$ Morse clusters, with the potential parameters given in Fig. 8, we estimate that $t_F^{\eta=2}=300$ fs for Coulomb explosion and $t_F^{\eta=2}=1200$ fs for fission. These time scales constitute the upper limits for the characteristic fragmentation times. In order to extract physically meaningful time scales for the nuclear dynamics, the data of Fig. 5 have to be corrected for the incubation times prior to the temporal onset of fragmentation, involving the intracluster excitation to the transition state. A cursory examination of the snapshots in Fig. 6 indicates that for cluster fission the incubation t_I for the initial formation of two fragments is $t_I \simeq 500$ fs, while for Coulomb explosion the onset of fragmentation is considerably shorter, being $t_I < 100$ fs. To provide a semiquantitative estimate of the time scales for fragmentation, we define a characteristic time scale $\tau_F^{\eta=2}$ for the doubling of the initial cluster radius (for $\eta=\ell/R_0=2$). This is given by $\tau_F^{\eta=2}=t_F^{\eta=2}-t_I$, where $t_F^{\eta=2}$ is the corresponding cluster doubling lifetime on the absolute time scale is subsequently corrected for the incubation time. For cluster fission the data of Figs. 5 and 7 result in $\tau_F^{\eta=2} \simeq 700$ fs, while for cluster Coulomb explosion $\tau_F^{\eta=2} \simeq 300$ fs. The longer time scale for cluster fission as compared to Coulomb explosion is $\tau_F^{\eta=2}(\text{fission})/\tau_F^{\eta=2}(\text{Coulomb explosion}) \simeq 2$.

These results can be rationalized in terms of simple kinematic models for the time scales of cluster Coulomb explosion[56,60,61] and of cluster fission.[56] For cluster Coulomb explosion of a cluster of initial radius R_0, the characteristic time for the attainment of a radius R is given by[60,61]

$$t(\xi) = t_0 Z(\xi), \tag{13}$$

where

$$\xi = R_0/R, \tag{13a}$$

$$Z(\xi) = [(1-\xi)^{1/2}/\xi] + (1/2)\ell n\left[\frac{1+(1-\xi)^{1/2}}{1-(1-\xi)^{1/2}}\right], \tag{13b}$$

$$t_0 = 0.931 q^{-1}(m/\rho)^{1/2}, \tag{13c}$$

where q is the ionic charge (in e units), m is the ion mass (in amu), ρ is the initial number density (in Å^{-3}) of the initial cluster, while $t(\xi)$ and t_0 are given in femtoseconds. The cluster fission is described in terms of a two-center Coulomb system, which is isomorphous to the fission of a diatomic molecule.[56] We consider fission of a cluster with n constituents and an initial radius R_0 into two cluster fragments. Each of these fragments involves $n/2$ constituents and is characterized by a mass $nm/2$ and a radius $\bar{r}_0$, with $\bar{r}_0=R_0/2^{1/3}$, with the initial distance between the cluster fragments being $\tilde{R}_0=2^{2/3}R_0$. The time for the increase of this initial separation to the value of $\tilde{R}$ is derived from the diatomic model[56] by

$$t(\tilde{\xi}) = \tilde{t}_0 Z(\tilde{\xi}), \tag{14}$$

where

$$\tilde{\xi} = \tilde{R}_0/\tilde{R}. \tag{14a}$$

$Z(\tilde{\xi})$ is given by Eq. (13b) with $\tilde{\xi}$ replacing ξ and

$$\tilde{t}_0 = 1.905 \tilde{q}^{-1}\tilde{R}_0^{3/2}\tilde{\mu}^{1/2}, \tag{14b}$$

where $\tilde{q}=qn/2$ is the fragment mass, $\tilde{R}_0=2^{2/3}(3n/4\pi\rho)^{1/3}$, and $\tilde{\mu}=nm/4$ is the reduced mass of each fragment. From Eq. (14b) we estimate that

$$\tilde{t}_0 = 1.869 q^{-1}(m/\rho)^{1/2} \tag{14c}$$

with the same units as for Eq. (13c). From Eq. (14c) we infer that $\tilde{t}_0$ for fission is independent of the size of the cluster and of the fragments and differs from the coefficient t_0 for the Coulomb explosion, Eq. (13c), by a numerical coefficient. For the case of cluster radius doubling, when $\xi=\tilde{\xi}=1/2$ or when $\eta=\xi^{-1}=\tilde{\xi}^{-1}=2$, we can identify $\tau_F^{\eta=2}(\text{fission}) = \tilde{t}_0 Z(1/2)$ and $\tau_F^{\eta=2}(\text{Coulomb explosion}) = t_0 Z(1/2)$. From Eqs. (13), (13c), (14), and (14c) we then obtain that $\tau_F^{\eta=2}(\text{fission})/\tau_F(\text{Coulomb explosion}) = \tilde{t}_0/t_0 \simeq 2$.

From this analysis we infer that the characteristic lifetime for the doubling of the initial cluster radius is longer for cluster fission than for Coulomb explosion, with a twofold increase of $\tau_F^{\eta=2}$(fission) relative to $\tau_F^{\eta=2}$ (Coulomb explosion). This prediction is in accord with the foregoing analysis of the data of Figs. 6 and 8. The problem of fragmentation dynamics will be subjected to a detailed investigation in a forthcoming paper.[87]

V. CONCLUDING REMARKS

From this foregoing analysis two distinct fragmentation modes of multicharged clusters, i.e., fission and Coulomb explosion, were established:

(1) Fissibility parameter. $X=1$ marks the "transition" between cluster fission ($X<1$) and cluster Coulomb explosion ($X>1$), in accord with the 1884 criterion of Rayleigh.[67]
(2) Products. The fission process results in a small number of large charged clusters, while the Coulomb explosion yields a large number of small charged clusters.
(3) Spatial distribution. The fission is spatially anisotropic, while Coulomb explosion is spatially isotropic.
(4) Kinetic energies of fragments. For fission, the kinetic energies and the internal energies of the large fragments are high, with the total kinetic energy ΣE_{KE} being comparable to the total inner energy ΣE_{IN}. For Coulomb explosion the major energy content of the fragments is ΣE_{KE}, which is considerably larger than ΣE_{IN}.
(5) Fragmentation times. These are characterized by the cluster fragmentation times τ_F^{η} for η-fold spatial expansion of the initial cluster radius. The τ_F^{η} times are longer for cluster fission than for Coulomb explosion, with the difference (of about a numerical factor of 2) in the characteristic times originating from the distant spatial distributions of the fragments in the two cases. We also note that the incubation periods for the onset of fragmentation are longer ($\sim$500 fs) for cluster fission and much shorter for Coulomb explosion.

Our model calculations demonstrated the prevalence of finite temperature cluster fission for $X<1$, while beyond the fissibility limit, i.e., $X>1$, Coulomb explosion prevails. While our results pertain strictly to covalently bound molecular clusters, we expect that this basic distinction between the two fragmentation modes is applicable to a broad variety of systems where repulsive Coulomb interactions or pseudo-Coulomb[71] interactions render the system to be unstable. These systems belong to the following categories:

(i) Nuclei. In the realm of nuclear physics, the fissibility parameter is $X\simeq 0.7$ for ^{235}U and about $X=0.9$ for the newly discovered $Z=114$ element.[83] So, as is well known, fission is predominant in disintegration of nuclei. The cornerstone of nuclear physics, which rests on the LDM, was recently experimentally[84] and theoretically[85,86] extended to incorporate "liquid-gas" transitions of heavy nuclei at high internal energies, which results in novel fragmentation modes. These will be briefly discussed at the end of this section.
(ii) Droplets. For hydrogen-bonded liquid droplets fission was recorded for droplets of ethylene glycol for $X=0.7$ and for $X<1$.[68–70]
(iii) Metal clusters. For multiply charged metal clusters, the maximal value of $X=0.85\pm0.07$ was obtained for Na_n^{+2} clusters,[53,54] which exhibit fission. A new fragmentation pattern was experimentally recorded[39] by high-energy collision of Na_n clusters with Xe^{20+} ions, with the production of a large number of singly charged Na^+ ions, which marks Coulomb explosion of highly-charged Na_n clusters. Information from Monte-Carlo simulations on evaporation, fission, and multifragmentation of multicharged metal clusters[39] demonstrated that multifragmentation of Na_{70}^{Z+} clusters with $Z>8$ (which approximately corresponds to $X>1.8$) manifests Coulomb explosion into small fragments. These simulation results for multicharged metal clusters concur with the results of the present analysis for highly charged molecular clusters.
(iv) Highly-charged molecular clusters. Extreme multielectron ionization of molecular clusters, e.g., Xe_n, $(D_2)_n$, $(H_2O)_n$, $(D_2O)_n$, $(CH_4)_n$, $(CD_4)_n$, $(HI)_n$, and $(DI)_n$, in ultraintense laser fields (peak intensity $I=10^{15}$–10^{20} W cm^{-2}) results in a complete or partial stripping of all the electrons from the cluster, e.g., the production of $(D^+)_n$ (at $I>10^{17}$ W cm^{-2}), $[(D^+)_2O^{6+}]_n$ and $[(D^+)_4C^{+4}]_n$ at $I=10^{17}$–10^{18} W cm^{-2}, $[(D^+)_2O^{8+}]_n$ and $[(D^+)_4C^{6+}]_n$ at $I=10^{19}$ W cm^{-2}, $(Xe^{q+})_n$ with $q=26$, or $(D^+I^{q+})_n$ with $q=25$ at $I=10^{19}$ W cm^{-2}.[44–61,80–84] These extreme cluster charges $Z=nq$ result in $X\gg 1$, driving Coulomb explosion.[42–61,80–84,87]
(v) Ultracold optical molasses.[71] Three-dimensional optical molasses consisting of low-density (10^{11}–10^{12} cm^{-3}), ultracold ($T=10$–100 μK) clouds of neutral (R_b) atoms, subjected to a radiative trapping force, which results from emission and reabsorption of laser radiation in a finite volume.[71] This radiative trapping force is equivalent to interatomic Coulomb repulsive force, with an effective charge of $q_{\mathrm{eff}}=4\times10^{-5}$.[71,88] When the magnetic trap is suppressed, the cloud expands via the radiative trapping force. The restoring surface energy is expected to be negligibly small, so that one expects that $X\gg 1$ even for these low values of q_{eff}.[88] The nuclear dynamics of optical molasses manifests isotropic, radial spatial expansion in analogy with Coulomb explosion. The time scales $\tau_M\simeq 1$ ms for Rb ultracold, laser-irradiated clouds for the isotropic expansion of optical molasses is in accord with the theory of Coulomb explosion.

From this classification of the manifestation of Coulomb instability [systems (i)–(iv)] and pseudo-Coulomb instability [class (v)] in large, finite systems, the following conclusions emerge:

(1) The Rayleigh limit with $X<1$ is prevalent in nuclei [class (i)], liquid droplets [class (ii)], and low-charged clusters [class (iii)]. For highly ionized metal clusters [class (iii)], extremely ionized molecular clusters [class (iv)] and optical molasses [class (v)] $X>1$, the Rayleigh limit is transcended and Coulomb explosion occurs.
(2) The fissibility parameter X can be expressed by[37]

$$X=(Z^2/n)/(Z^2/n)_{\mathrm{cr}}, \tag{15}$$

where

$$(Z^2/n)_{\mathrm{cr}}=4(4\pi\gamma r_0^2)/(e^2/r_0) \tag{15a}$$

representing the ratio between surface and Coulomb energies on the single constituent scale (Sec. I). From the LDM analysis of Sec. III we can present the X parameter for a $(A^+)_n$ Morse cluster by Eqs. (15) and (15a) with $\gamma=a_s/4\pi r_0^2$. Alternatively, one can use Eq.

TABLE IV. The normalization factor $(Z^2/n)_{cr}$ for the fissibility parameter $X=(Z^2/n)/(Z^2/n)_{cr}$.

Systems	γ(erg cm^{-2})	r_0(Å)	$(Z^2/n)_{cr}$	Source	References
Nuclei	⋯	10^{-5}	52	Eq. (15b)	[a]
Liquid droplets	70	3	0.40	Eq. (15a)	[b]
Metal clusters	⋯	1.7–3.1	0.4–1.1	Eq. (15b)	[c]
Liquid elemental clusters	12.7	3	0.07	Eq. (15a)	[d]
Multicharged Morse clusters					
(s) type	⋯	3	$3.87D$	Eq. (15b)	[e]
(ℓ) type		1	$36.4D$		
Optical molasses	0	10^4	0	Eq. (15a)	[f]

[a]$(Z^2/n)_{cr}$ from Ref. 66.
[b]γ surface tension of water from Ref. 90. $(Z^2/n)_{cr}$ from Ref. 37.
[c]$(Z^2/n)_{cr}$ from Ref. 37.
[d]Surface tension of liquid Ar at $T=87$ K, footnote b.
[e]Present work. $(s)\alpha=3$ Å^{-1}, $R_e=3$ Å, $q=1$, $(\ell)\alpha=1$ Å^{-1}, $R_e=2$ Å; D is the pair dissociation energy.
[f]Reference 71.

(8a) with $Z^2/n \equiv n$ expressing X, Eq. (13), in terms of

$$(Z^2/n)_{cr} = 2a_s/a_c. \tag{15b}$$

In Table IV we assemble the values of γ together with the $(Z^2/n)_{cr}$ normalization factors estimated from Eqs. (15a) and (15b).

(3) The Rayleigh limit ($X=1$) transcended in two situations. These involve either a marked enhancement of the Coulomb energy, as is the case for extremely ionized molecular clusters [case (iv)], or a dramatic reduction of the surface energy, as is the case for the expansion of optical molasses [case (v)].

We conclude this discussion with two comments pertaining to the LDM for the instability of multicharged large systems and the implications of the LDM for fragmentation modes beyond fission. The fission process is usually connected with the liquidlike behavior of the finite system. A real life example involves the fission of doubly charged metal clusters, which is related to the fact that they exist in the liquid state.[37] However, the fission process is not exclusively characteristic of the liquid drop. Fission may be realized in solid (rigid) finite systems under special conditions. In considering the fragmentation patterns of extremely multicharged Morse clusters studied herein, we have to take into account that these clusters behave like solid-state bodies. The first piece of evidence for this solid-state behavior of the Morse-Coulomb clusters lies in their response to outer force. We applied a weak outer stretch force to the cluster. In the case of a liquid body such a force would result in an elongation of the cluster. In our case, such a force was found to generate oscillations, which are typical for a solid-state body. In the A_{55}^{55+} cluster with the Morse-potential parameters $\alpha=3$ Å^{-1}, $R_e=3$ Å, and $D=8$ eV, the frequency of these oscillations was found to be 5.0–5.5 ps^{-1}. The second piece of evidence for the solid-state "phase" of the Morse cluster emerges from the ion trajectories in the molecular dynamics, which do not indicate any migration of the ions prior to fragmentation. It appears that the classification of the fragmentation channels of large finite systems goes beyond the LDM and is applicable also for rigid systems provided that the Coulomb and surface energies are properly estimated.

The traditional application of the LDM for the description of fission of multicharged finite systems was recently extended in the realm of nuclear physics.[84–86] This interesting development pertains to the "evaporation" of heavy nuclei at high energies. By high-energy excitation of Au^{197} it was experimentally demonstrated[84] that spatially isotropic fragmentation, with the abundance of small nuclear fragments, i.e., dimers, trimers and tetramers, takes place above an energy threshold of ~8 MeV. These novel phenomena were attributed to the evaporation of the liquid drop.[84] Concurrent theoretical work[85,86] showed that the observed number and the size distribution of the small fragments matched the predictions of general statistical theories of (first-order) phase transitions in a liquid droplet.[89] The nuclear evaporation process was described[85,86] by the critical exponents, the critical point and the surface energy coefficient for finite nuclear matter. It will be interesting to explore the relation between Coulomb explosion of extremely multicharged molecular clusters and finite-size scaling of phase transitions for liquid-gas evaporation.[89] In the present work we have shown that for the spatially isotropic Coulomb explosion of large multicharged Morse-Coulomb clusters (Figs. 4 and 5), small fragments (i.e., from monomers to tetramers) are formed. This cluster disintegration seems to bear analogy to the evaporation of liquid droplets[89] and of nuclei.[84–86] It will be interesting to apply the finite-size-scaling theory[89] for first-order phase transitions to explore the onset of Coulomb explosion of multicharged large clusters, establishing dynamic-thermodynamic relations for fragmentation.

ACKNOWLEDGMENT

This article is dedicated to the memory of Richard Bersohn.

[1] R. Kubo, J. Phys. (Paris) **38**, 270 (1977).
[2] J. Friedel, J. Phys. (Paris) **38**, 1 (1977).
[3] See Special Issue on *Molecular Clusters* [Chem. Phys. **239**, 1 (1998)].
[4] *Structure and Dynamics of Clusters*, edited by T. Kondow, K. Kaya, and A. Terasaki (University Press, Tokyo, 1996).
[5] M. Astnie Hoffmann, G. Wrigge, B. V. Issendorff, J. Müller, G. Gantefor, and H. Haberland, *Proceedings of the Tenth International Symposium of Small Particles and Inorganic Clusters*, Altanta, Georgia, 11–15 October

2000, edited by C. Yannouleas and U. Landman, Eur. Phys. J. D 16, 9 (2001).
[6] *Theory of Atomic and Molecular Clusters*, edited by J. Jellinek (Springer, Berlin, 1999).
[7] *Clusters of Atoms and Molecules*, edited by H. Haberland (Springer, Berlin, 1994).
[8] J. Jortner, Z. Phys. D: At., Mol. Clusters **24**, 247 (1992).
[9] J. Jortner, Z. Phys. Chem. (Munich) **184**, 283 (1994)
[10] J. Jortner, J. Chim. Phys. Phys. **92**, 205 (1995).
[11] P. Alivisatos, Science **271**, 933 (1996).
[12] B. Von Issendorff and O. Cheshnovsky, Annu. Rev. Phys. Chem. **56**, 549 (2005).
[13] V. Bonacic-Koutecky and R. Mitric, Chem. Rev. **105**, 11 (2005).
[14] J. Jortner and N. C. R. Rao, Pure Appl. Chem. **74**, 1491 (2002).
[15] *Quantum Phenomena in Clusters and Nanostructures*, edited by S. Khanna and A. W. Castleman (Springer, Berlin, 2002).
[16] E. G. Robertson and J. P. Simons, Phys. Chem. Chem. Phys. **3**, 1 (2001).
[17] K. Sattler, J. Mühlbach, O. Echt, P. Pfau, and E. Recknagel, Phys. Rev. Lett. **47**, 160 (1981).
[18] D. Kreisle, O. Echt, M. Knapp, E. Recknagel, K. Leiter, T. D. Märk, J. J. Sáenz, and J. M. Soler, Phys. Rev. Lett. **56**, 1551 (1986).
[19] P. Scheier and T. D. Märk, Chem. Phys. Lett. **136**, 423 (1987).
[20] M. Lezius and T. D. Märk, Chem. Phys. Lett. **155**, 496 (1989).
[21] A. J. Stace, P. G. Lethbridge, and J. K. E. Upham, J. Phys. Chem. **93**, 333, (1989).
[22] S. Sugaron, A. Tamura, and Y. Ishii, Z. Phys. D: At., Mol. Clusters **12**, 213 (1989).
[23] C. Bréchignac, Ph. Cahuzac, J. Leygnier, and J. Weiner, J. Chem. Phys. **90**, 1492 (1989).
[24] M. Lezius, P. Scheier, A. Stamatovic, and T. D. Märk, Chem. Phys. **91**, 3240 (1989).
[25] I. Katakuse, H. Ito, and A. Ichihara, Int. J. Mass Spectrom. Ion Process. **97**, 47 (1990).
[26] C. Bréchignac, Ph. Cahuzac, F. Carliez, and M. de Frutos, Phys. Rev. Lett. **64**, 2893 (1990).
[27] W. A. Saunders and N. Dam, Z. Phys. D: At., Mol. Clusters **20**, 111 (1991).
[28] C. Bréchignac, Ph. Cahuzac, N. Kebaili, J. Leignier, and A. Sarfati, Phys. Rev. Lett. **68**, 3916 (1992).
[29] N. G. Gotts, P. G. Lethbridge, and A. J. Stace, J. Chem. Phys. **96**, 408 (1992).
[30] H. J. Krappe, Z. Phys. D: At., Mol. Clusters **23**, 269 (1992).
[31] W. A. Saunders, Phys. Rev. A **46**, 7028 (1992).
[32] C. Bréchignac, Ph. Cahuzac, F. Carlier, and M. de Frutos, Phys. Rev. B **49**, 2825 (1994).
[33] A. Goldberg, I. Last, and T. F. George, J. Chem. Phys. **100**, 8277 (1994).
[34] U. Näher, S. Frank, N. Malinowski, U. Zimmermann, and T. P. Martin, Z. Phys. D: At., Mol. Clusters **31**, 191 (1994).
[35] F. Chandezon, C. Guet, B. A. Huber, M. Jalabert, E. Maurel, E. Monnand, C. Ristori, and J. C. Rocco, Phys. Rev. Lett. **74**, 3784 (1995).
[36] C. Bréchignac, Ph. Cahuzac, M. de Frotos, N. Kebaili, and A. Sarfati, Phys. Rev. Lett. **77**, 251 (1996).
[37] U. Näher, S. Bjornholm, S. Fraundorf, F. Gracias, and C. Guet, Phys. Rep. **285**, 245 (1997).
[38] C. Guet, X. Biquard, P. Blaise, S. A. Blundell, M. Gross, B. A. Huber, D. Jalabert, M. Maurel, L. Plague, and J. C. Rocco, Z. Phys. D: At., Mol. Clusters **40**, 317 (1997).
[39] O. Shapiro, P. J. Kunz, K. Möhring, P. A. Hervieux, D. H. F. Gross, and M. E. Madjet, Z. Phys. D: At., Mol. Clusters **41**, 219 (1997).
[40] C. Bréchignac, Ph. Cahuzac, N. Kébaili, and J. Leygnier, Phys. Rev. Lett. **81**, 4612 (1998).
[41] N. Saito, K. Koyama, and M. Tanimoto, Chem. Phys. Lett. **300**, 262 (1999).
[42] J. Purnell, E. M. Snyder, S. Wei, and A. W. Castleman, Jr., Chem. Phys. Lett. **229**, 333 (1994).
[43] O. Zhong and A. W. Castleman, Jr., Chem. Rev. (Washington, D.C.) **100**, 4039 (2000).
[44] T. Ditmire, T. Donnelly, A. M. Rubenchik, R. W. Falcone, and M. D. Perry, Phys. Rev. A **53**, 3379 (1996).
[45] T. Ditmire, J. W. G. Tisch, E. Springate, M. B. Mason, N. Hay, R. A. Smith, J. Marangos, and M. H. R. Hutchinson, Nature (London) **386**, 54 (1997).
[46] T. Ditmire, J. W. G. Tisch, E. Springate, M. B. Mason, N. Hay, J. P. Marangos, and M. H. R. Hutchinson, Phys. Rev. Lett. **78**, 2732 (1997).
[47] M. H. R. Hutchinson, T. Ditmire, E. Springate, J. W. G. Tisch, Y. L. Shao, M. B. Mason, N. Hay, and J. P. Marangos, Philos. Trans. R. Soc. London, Ser. A **356**, 297 (1998).
[48] T. Ditmire, E. Springate, J. W. G. Tisch, Y. L. Shao, M. B. Mason, N. Hay, J. P. Marangos, and M. H. R. Hutchinson, Phys. Rev. A **57**, 369 (1998).
[49] E. Springate, N. Hay, J. W. G. Tisch, M. B. Mason, T. Ditmire, M. H. R. Hutchinson, and J. P. Marangos, Phys. Rev. A **61**, 063201 (2000).
[50] J. Kou, N. Nakashima, S. Sakabe, S. Kawato, H. Ueyama, T. Urano, T. Kuge, Y. Izawa, and Y. Kato, Chem. Phys. Lett. **289**, 334 (1998).
[51] V. P. Krainov and M. B. Smirnov, Phys. Rep. **370**, 237 (2002).
[52] M. Lezius, S. Dobosh, D. Normand, and M. Schmidt, Phys. Rev. Lett. **80**, 261 (1998).
[53] J. Daligault and C. Guet, Phys. Rev. A **64**, 043203 (2001).
[54] F. Chandezon, S. Tomita, D. Cornier, P. Grubling, C. Guet, H. Lebius, A. Pesnelle, and B. A. Huber, Phys. Rev. Lett. **87**, 153402 (2001).
[55] F. Chandezon, T. Bergen, A. Brenac, C. Guet, B. A. Huber, H. Lebius, and A. Pesnelle, Phys. Rev. A **63**, 051201 (2001).
[56] I. Last, I. Schek, and J. Jortner, J. Chem. Phys. **107**, 6685 (1997).
[57] I. Last and J. Jortner, Phys. Rev. A **60**, 2215 (1999).
[58] I. Last and J. Jortner, Phys. Rev. A **62**, 013201 (2000).
[59] I. Last and J. Jortner, J. Chem. Phys. **120**, 1336 (2004).
[60] I. Last and J. Jortner, J. Chem. Phys. **120**, 1348 (2004).
[61] I. Last and J. Jortner, J. Chem. Phys. **121**, 8329 (2004).
[62] N. Bohr and J. A. Wheeler, Phys. Rev. **56**, 426 (1939).
[63] L. Meitner and O. R. Frisch, Nature (London) **143**, 239 (1939).
[64] S. Frenker and N. Metropolis, Phys. Rev. **72**, 914 (1947).
[65] P. Möller, D. G. Madland, A. J. Sierk, and A. Iwamoto, Nature (London) **409**, 785 (2001).
[66] P. Heyde, *Basic Ideas and Concepts in Nuclear Physics* (IOP, Bristol, 1994).
[67] L. Lord Rayleigh, Philos. Mag. **14**, 184 (1884).
[68] D. C. Taflin, T. I. Ward, and E. J. Davis, Langmuir **5**, 376 (1989).
[69] J. F. Widman, C. L. Arrdahl, and E. J. Davis, Aerosol Science Technology **27**, 636 (1979).
[70] D. Duft, H. Lebius, B. A. Huber, C. Guet, and T. Leisner, Phys. Rev. Lett. **89**, 084503 (2002).
[71] L. Pruvost, I. Serri, H. T. Duong, and J. Jortner, Phys. Rev. A **61**, 053408 (2000).
[72] L. Köller, M. Schumacher, J. Köhn, S. Teuber, J. Tiggesbäumker, and K. H. Meiwes-Broer, Phys. Rev. Lett. **82**, 3783 (1999).
[73] M. Schumacher, S. Teuber, L. Köller, J. Köhn, J. Tiggesbäumker, and K. H. Meiwes-Broer, Eur. Phys. J. D **9**, 411 (1999).
[74] T. Döppner, S. Teuber, M. Schumacher, J. Tiggesbäumker, and K. H. Meiwes-Broer, Int. J. Mass. Spectrom. **192**, 387 (1999).
[75] J. W. G. Tisch, N. Hay, E. Springate, E. T. Gumbrell, M. H. R. Hutchinson, and J. P. Marangos, Phys. Rev. A **60**, 3076 (1999).
[76] J. Zweiback, R. A. Smith, T. E. Cowan, G. Hays, K. B. Wharton, V. P. Yanovsky, and T. Ditmire, Phys. Rev. Lett. **84**, 2634 (2000).
[77] J. Zweiback, T. E. Cowan, R. A. Smith, J. H. Hurtlay, R. Howell, C. A. Steinke, G. Hays, K. B. Wharton, J. K. Krane, and T. Ditmire, Phys. Rev. Lett. **85**, 3640 (2000).
[78] I. Last and J. Jortner, Phys. Rev. Lett. **87**, 033401 (2001).
[79] I. Last and J. Jortner, Phys. Rev. A **64**, 063201 (2001).
[80] I. Last and J. Jortner, J. Chem. Phys. **120**, 1348 (2004).
[81] I. Last, Y. Levy, and J. Jortner, Proc. Natl. Acad. Sci. U.S.A. **99**, 9107 (2002).
[82] Y. Levy, I. Last, and J. Jortner (unpublished).
[83] Yu. Ts. Oganessian, A. V. Yeremin, A. G. Popek *et al.* Nature (London) **400**, 242 (1999).
[84] C. Seife, Science **295**, 603 (2002).
[85] J. B. Elliot, L. G. Moretto, L. Phair *et al.*, Phys. Rev. Lett. **88**, 042701 (2002).
[86] M. K. Berkenbusch, W. Bauer, K. Dillman *et al.*, Phys. Rev. Lett. **88**, 022701 (2002).
[87] I. Last and J. Jortner, Proc. Natl. Acad. Sci. U.S.A. **102**, 1291 (2005).
[88] L. Pruvost (private communication).
[89] M. E. Fischer, Physica (New York) **3**, 255 (1967).
[90] J. R. Partington, *An Advanced Treatise on Physical Chemistry* (Longmans, London, 1951).